23rd International Symposium on Mathematical Theory of Networks and Systems
Hong Kong University of Science and Technology, Hong Kong, July 16-20, 2018

General Inverse Sensor Model for Probabilistic Occupancy Grid Maps using Multi-Target Sensors

Roxana Dia*, Suzanne Lesecq*, Julien Mottin* and Diego Puschini*

***Abstract*— Environment perception is a crucial task for safe navigation of robots. It relies on the robust interpretation of noisy sensor measurements. To represent the state of the surrounding environment, probabilistic Occupancy Grids are commonly used. They are built using a Bayesian inference procedure which estimates the occupancy probability of each cell in the grid from sensor readings. However, the complexity of such a procedure is exponentially increasing with the number of cells, especially when sensor readings are caused by multiple targets simultaneously. To overcome this difficulty, we propose a novel approach to handle multi-target sensors. It is based on a sectoral decomposition of their Field-Of-View under the nearest-target hypothesis, which breaks down the complexity to a linear one. Finally, a realistic implementation of the proposed formulation is presented, and an experimental construction of occupancy grids is discussed.**

I. INTRODUCTION

Mobile robots require building a representation of their environment to autonomously and safely navigate. Several spatial representations have been used for this purpose [1], [2], [3], [4]. *Occupancy Grids* (OGs) , originally introduced in [1], seem to be the most commonly used representation in this domain. OGs are composed of a finite number of cells corresponding to a partition of the space that surrounds the robot. Each cell is associated to a qualitative information about its state which reflects the certainty of being occupied given sensor measurements. Three types of OGs exist, namely, probabilistic OGs [5], evidential OGs [6] and fuzzy OGs [7]. The difference lies in the way this information is computed. The model used to compute the qualitative information is the so-called *Inverse Sensor Model* (ISM), also known as the posterior model. It enables to estimate occupied and empty regions, given sensor measurements. Sensor uncertainty is captured by a probability density function, also known as the *Sensor Model* (SM). The SM can be determined experimentally *via* several tests that permit to model the behavior of the sensor in different situations and conditions. It can also be determined theoretically from a knowledge of the physics principles behind the sensor.

In this paper, multi-target sensors are considered, i.e. sensors which have a large Field-Of-View (FOV) (see Fig. 1a) and whose measurements vary depending on the number of targets present in their FOV and the Cross Section (CS) of the targets considered. Their behavior is different from narrow FOV sensors, often called single-target sensors. For these narrow FOV sensors, mostly the nearest target to the sensor is supposed to generate the measurement and its CS does not have much influence since its FOV is considered infinitely narrow (see Fig. 1b). Basically, in the case of multi-target sensors, the problem is that the Bayesian inference procedure requested for the ISM evaluation requires an enumeration of all possible environment states. Therefore, the computational complexity is exponential, becoming intractable in large OGs. Several approaches have been proposed in order to reduce the computational complexity of the ISM [8] [9] [10] [11] [12]. However, these approaches introduced some approximations in the ISM formulation or they gave a direct formulation of the ISM without employing the SM, or they reduced the complexity for single-target sensors and therefore can't be applied to multi-target sensors.

From a theoretical point of view, it is of great interest to keep the link between the SM and the ISM [10]. Consequently, the present paper proposes a *linear-complexity* implementation of the ISM for multi-target sensors that keeps this link. The implementation decomposes the FOV in sectors for the ISM computation. It it is based on the nearest-target hypothesis, i.e. the measurement provided by the sensor is supposed to be caused by the closest obstacle to the sensor (or several obstacles if they are at the same closest distance to the sensor) and it is influenced by the obstacle CS and its angular position (their equivalent CS and their angular position, respectively).

The paper is organized as follows. Section II gives a brief introduction to the basic terminologies and the mathematical background, exposes the limitations encountered by previous approaches and discusses in details the nearest-target hypothesis. The definition of the SM based on the nearest-target hypothesis is then presented in section III while section IV covers the direct formulation of the ISM. Section V details the implementation of the sectoral decomposition. Finally, results for this new formulation based on the sectoral decomposition technique are presented in section VI.

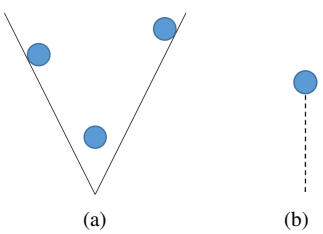

Fig. 1: Illustration of a multi-target FOV sensor (a) and of a single-target FOV sensor (b).

*Univ. Grenoble Alpes, CEA, Leti, F-38000 Grenoble, France. This work has been partially funded by the EUREKA CATRENE TRACE project and by the European Union Horizon 2020 Research and Innovation programme under grant agreement 730953-INSPEX.

II. Motivation

In this section, we first recall the mathematical definitions of the SM and the ISM in II-A. Then, we expose the computational burdens of the ISM evaluation for multi-target sensors in II-B. Finally, subsection II-C shows that the nearest-target hypothesis is already valid for some commercial sensors.

A. Mathematical Formulation and Terminology

$\mathcal{G}$ is the OG partitioned into a finite number of N disjoint cells c_i , $i = 0, \dots, N-1$. Each cell c_i is associated to its state s_i, where $s_i = o(c_i)$ if cell c_i is occupied, and $s_i = e(c_i)$ if c_i is empty. z denotes the sensor response toward a specific grid configuration G. The SM is the conditional probability distribution $p(z|G)$ that z occurs given a specific configuration G of $\mathcal{G}$. The parameters that appear in the SM formulation may vary from one sensor to the other.

For a single-target sensor, a convenient representation of the SM is given by $p(z|x)$ where x is the distance from the sensor to its closest obstacle. The single-target hypothesis implies that $p(z|G)$ can be expressed as $p(z|x(G))$, where $x(G)$ is the distance to the first occupied cell in G. Hence, the distribution $p(z|G)$ can be computed with a linear complexity for single-target sensors [10]. However, for a multi-target sensor, a similar simplification does not hold because multiple objects at the same distance can be detected in a single sensor reading. The sensor output therefore relates to the combination of the occupancy state of the corresponding cells. Both situations greatly differ and the construction of the multi-target SM will be discussed in section III.

The ISM is represented by the conditional probability of occupancy of each cell, given the measurement z. Assume that the occupancy of different cells is conditionally independent with respect to z. Then, the ISM is given by $P(o(c_i)|z)$, $i = 0, \dots, N-1$. The methodology proposed by Elfes [13] to deduce the ISM from the SM is based on the Bayes' theorem:

$$P(o(c_i)|z) = \frac{p(z|o(c_i)) \cdot P(o(c_i))}{p(z)} \tag{1}$$

From the decomposition on the two complementary events $o(c_i)$ and $e(c_i)$, (1) becomes:

$$P(o(c_i)|z) = \frac{p(z|o(c_i)) \cdot P(o(c_i))}{p(z|o(c_i)) \cdot P(o(c_i)) + p(z|e(c_i)) \cdot P(e(c_i))} \tag{2}$$

$P(o(c_i))$ and $P(e(c_i))$ evaluate the prior information about the occupancy of cell c_i. Equation (2) requires the computation of $p(z|e(c_i))$ and $p(z|o(c_i))$. It is then feasible to compute $p(z|s_i)$, $s_i \in \{o(c_i), e(c_i)\}$ from the SM. From the total probability law applied over all the possible grid configurations, it comes:

$$p(z|s_i) = \sum_{G_k^{s_i}} p(z|G_k^{s_i} \wedge s_i) \cdot P(G_k^{s_i}|s_i) \tag{3}$$

where $G_k^{s_i}$ refers to a grid that has no state information for cell c_i: $G_k^{s_i} = (s_0, \dots, s_{i-1}, s_{i+1}, \dots, s_{N-1})$ and $G_k^{s_i} \wedge s_i = (s_0, \dots, s_{i-1}, s_i, s_{i+1}, \dots, s_{N-1})$. Hence, $G_k^{s_i} \wedge s_i$ represents the configuration of a grid where the state of cell c_i is set to s_i and the state of the other cells are enforced in $G_k^{s_i}$. Since $G_k^{s_i}$ is independent of s_i, (3) can be written as:

$$p(z|s_i) = \sum_{G_k^{s_i}} p(z|G_k^{s_i} \wedge s_i) \cdot P(G_k^{s_i}) \tag{4}$$

Although $p(z|G_k^{s_i} \wedge s_i)$ can be derived from SM evaluations, one can notice that the number of possible configurations $G_k^{s_i}$ in (4) is 2^{N-1}. In the case of a multi-target sensor, this leads to an exponential computation.

B. Analysis of Previous Approaches

As described in II-A, the theoretical solution to the ISM problem has an exponential complexity. To overcome the implementation burden, several approaches were proposed in the literature. They either introduced some approximations in the formulation or they developed a different methodology for building the ISM. For example, [10], [11], [12] apply the single-target hypothesis to compute $p(z|o(c_i))$ and $p(z|e(c_i))$ in (2). However, this would result in incorrect occupancy estimates for a multi-target sensor. Consider for instance a radar with a large FOV, and two grid configurations G_1 and G_2, where G_1 contains a unique occupied cell in the sensor FOV at a known distance d, while in G_2, all the cells located at distance d are occupied. The single-target hypothesis implies that $p(z|G_1)$ must be equal to $p(z|G_2)$, which intuitively contradicts the specular behavior of a radar. Moreover, the resulting ISM would reflect only the free space, but not the occupancy.

Another approach consists in a direct formulation of the ISM given a sensor measurement [8]. The occupancy of cells located outside the measurement range of the sensor FOV or behind a predefined distance are not updated: they are kept equal to their prior value. Cells that are within a predefined interval of the detected range are supposed occupied and their occupancy probability is updated. Finally, cells located in a shorter range than the sensor measurement are supposed empty. Such a parametric approximation of the ISM cannot be theoretically assessed, and the choice of its parameters has to be verified experimentally. In addition, it breaks the link between the SM and the ISM.

A third approach proposed in [9] supposes that the probability of occupancy $P(o(c_i)|z)$ is given by:

$$\frac{p(z|o(c_i)) \cdot P(o(c_i))}{p(z|o(c_i)) \cdot P(o(c_i)) + [1 - p(z|o(c_i))] \cdot P(e(c_i))} \tag{5}$$

However, $p(z|o(c_i))$ is not equal to $1 - p(z|e(c_i))$ in general. Moreover, the SM in [9] does not take into account the effect of other possibly occupied cells in the sensor FOV.

Finally, Thrun *et al.* [14] use a forward SM and apply the Expectation Maximisation technique to find the adequate map to a sensor measurement. Then, they compute the occupancy probability in each cell. This approach suffers from a complex computation and it does not always lead to a unique optimum.

To the best of our knowledge, there is no solution in the literature that explicitly keeps the link between the SM and the ISM for multi-target sensors. This paper presents a general formulation of the ISM under the nearest-target hypothesis that guarantees this link and proposes a reasonable linear-complexity implementation of the ISM by applying a sectoral decomposition of the sensor FOV. Table I compares previous approaches with our solution regarding the computational complexity, the link between the SM and the ISM and the application to multi-target sensors.

TABLE I: Comparison between existing approaches and the proposed solution.

Approach	Linear complexity	Maintains the link between the SM and ISM	Relevant to multi-target sensors
[12]	Yes	Yes	No
[11]	Yes	Yes	No
[10]	Yes	Yes	No
[8]	Yes	No	Yes
[9]	No	Yes	No
[14]	No	No	Yes
The present approach	Yes	Yes	Yes

C. Nearest-target hypothesis

The solution proposed here is rooted in the nearest-target hypothesis. This latter relies on the fact that the measurement provided by the sensor is supposed to be caused by the closest obstacle to the sensor (or by several obstacles if they are at the same closest distance to the sensor). As it will be shown in section III-B, this measurement is influenced by the obstacle CS (their equivalent CS respectively) and its (their) angular position.

The nearest-target behavior can be found in different range sensors already on the market. Several commercial sensors that embed Signal Processing (SP) to provide only one range measurement corresponding to the distance to the nearest obstacle(s) verify this hypothesis. For instance, each detector of the Vu8/M16 from LeddarTech presents such a behavior [15] [16]. In the same way, this hypothesis has been verified for sensors VL53L0X from STM [17] and TeraRanger ONE from Terabee [18]. Other range sensors provide raw data and further SP is implemented (either provided by the manufacturer or developed by the user) to compute the distances to the targets. Then, depending on the SP implemented, one can extract the smallest distance for each scanning direction and therefore the nearest-target hypothesis can be guaranteed. For instance, the radar transceiver BGT24Axx [19] together with the AURIX processor from Infineon [20] or the cocoon radar from NXP (transceiver MR3003 with processor S32R27) [21] can satisfy the nearest-target hypothesis, depending on the SP techniques implemented in their respective processor.

III. Probabilistic sensor model

Under the nearest-target hypothesis, the sensor measurement roots in 2 causes: either it is caused by the target(s) located at the closest distance to the sensor or by a missed detection. Both cases can be associated to a probability of detection p_D and of missed detection p_{MD}, respectively.

Subsection III-A briefly explains how the angular position of the target in the sensor FOV and its CS may influence these probabilities. Subsection III-B shows how these factors will interfere in the computation of these two probabilities. The mathematical formulation of the SM used in the present paper is also given. This model has been validated in [22]. Please note that the CS of a target is defined here as the measure of a target ability to reflect the signal in the direction of the sensor depending *only on the relative area covered by the target with respect to the sensor aperture and its absolute size*. Other factors that may impact the CS (such as the material of which the target is made) are not considered.

A. Factors Impacting the SM

First, the angular position is expected to play a role in the detection. A target located in the sensor FOV axis at distance x (Fig. 4a) will more likely be detected in comparison to the situation where it is located towards the side of the sensor FOV at the same distance (Fig. 3a), generating then a higher p_D and a smaller p_{MD}.

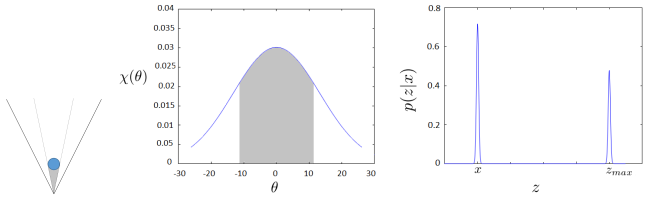

(a) (b) (c)

Fig. 2: (a): position of the target in the sensor FOV with Cross Section in gray. (b): angular uncertainty function χ where the gray shaded area corresponds to $P_D = 0.6$. (c): associated SM, x: distance from target to sensor.

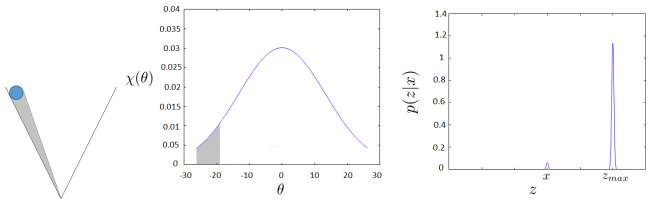

(a) (b) (c)

Fig. 3: Same as Fig. 2 with $P_D = 0.05$

A second impacting factor is the target CS, which seems neglected in the literature. For example, the target in Fig. 2a has a larger CS than the one in Fig. 4a even if both targets are identical in shape. The distances from the sensor to these targets are indeed different, leading to a different relative covered area for both targets with respect to the sensor aperture. Hence, the target in Fig. 2a will more likely

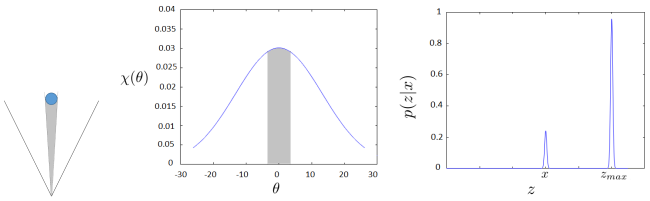

(a) (b) (c)

Fig. 4: Same as Fig. 2 with $P_D = 0.2$

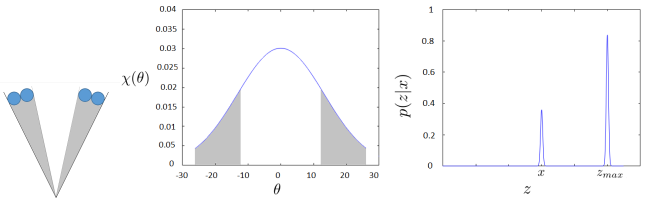

(a) (b) (c)

Fig. 5: Same as Fig. 2 with $P_D = 0.3$

reflect the signal emitted by the sensor than the one in Fig. 4a, yielding a higher P_D. A second example is illustrated in Fig 5a and Fig. 3a. Targets in Fig. 5a have a larger combined CS than the target in Fig. 3a. This time, the variation of the CS is caused by the absolute size of these targets.

Finally, one should note that the angular position and the CS have an interacting effect on the detection. For instance targets in Fig. 5a have a larger combined CS than the target in Fig. 4a. However, it cannot be directly stated that they have a higher P_D. In fact, targets in Fig. 5a are located at a poor reflecting area (towards the side of the sensor FOV). On the contrary, the target in Fig. 4a is located on the sensor FOV axis. It will be shown hereafter how both, the CS and the angular position, are considered in the mathematical expressions of P_D and P_{MD}.

B. Formulation of the Sensor Model

Consider $T = \{t_i; i = 1, ..., N_T\}$ the set of N_T targets located in the sensor FOV verifying $r(t_1) \leq r(t_2) \leq ... \leq r(t_{N_T})$, where $r(.)$ is the distance to the sensor. Denote $\Gamma(T) = \{t_1, ..., t_M\}$ the set of the M nearest targets located at the same smallest distance r^* with:

$$r^* = r(t_1) = r(t_2) = ... = r(t_M) \tag{6}$$

The SM is represented by the probability distribution function $p(z|T)$ where z is the sensor measurement. Since the nearest-target hypothesis is applied, the SM is simplified to $p(z|\Gamma(T))$. If the two probabilities P_D and P_{MD} associated to $\Gamma(T)$ are known, and taking into account the discussion above where the measurement is supposed to be caused by either the nearest target(s) or a missed detection, a convenient formulation of the SM is given by:

$$p(z|\Gamma(T)) = \frac{P_D}{\sigma_{r^*}\sqrt{2\pi}} e^{\frac{-(z-r^*)^2}{2{\sigma_{r^*}}^2}} + \frac{P_{MD}}{\hat{\sigma}\sqrt{2\pi}} e^{\frac{-(z-z_{max})^2}{2\hat{\sigma}^2}} \tag{7}$$

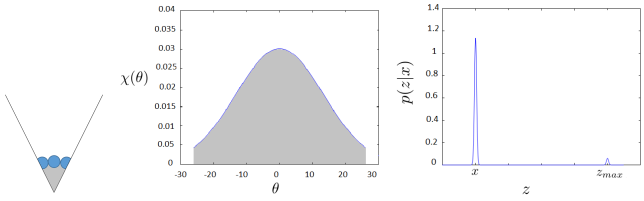

(a) (b) (c)

Fig. 6: Same as Fig. 2 with $P_D = 0.95$

where z_{max} is the maximum range returned by the sensor when there is a missed detection. Here, the sensor is supposed to have a Gaussian model and σ_{r^*} and $\hat{\sigma}$ are the standard deviations in the case of detection and missed detection respectively.

If P_D is known, one can directly deduce P_{MD} because these probabilities are associated to two complementary events and $P_{MD} = 1 - P_D$. Thus, only the formulation of P_D is now detailed, taking into account the discussion in subsection III-A.

For $i \in \{1, ..., M\}$, denote $\Omega(t_i)$ the CS of target t_i within the sensor FOV. From now on, and without lack of generality, the study is restricted to the two dimensional space. Then, the CS is restrained between two angular beams $\theta_{min}(t_i)$ and $\theta_{max}(t_i)$. Thus $\Omega(t_i)$ can be written as:

$$\Omega(t_i) = [\theta_{min}(t_i), \theta_{max}(t_i)] \tag{8}$$

This interval accounts for the CS and the angular position of the target at the same time. We also define $\Omega(\Gamma(T))$ as:

$$\Omega(\Gamma(T)) = \bigcup_{t \in \Gamma(T)} \Omega(t) \tag{9}$$

Notice that if $\Omega(\Gamma(T)) = [-\alpha/2, \alpha/2]$, where α is the width of the sensor FOV, then P_D takes its maximum value, denoted by P_D^{max} (Fig. 6). In fact, in this case the nearest target(s) has (have) the maximum possible CS within the sensor FOV. Therefore, it has (they have) the maximum reflection rate.

In order to determine the general formulation of P_D, and taking into account the value of P_D^{max}, we proceed as follows. First, we define σ^* as the solution over all $\sigma \in \mathbb{R}^{*+}$ verifying the following equation:

$$\int_{-\alpha/2}^{\alpha/2} \frac{1}{\sigma\sqrt{2\pi}} e^{\frac{-\theta^2}{2\sigma^2}} \, d\theta = P_D^{max} \tag{10}$$

σ^* can be found by noticing that (10) is equivalent to:

$$P(|\theta| < \frac{\alpha}{2}) = P_D^{max} \tag{11}$$

where θ follows a normal distribution $\mathcal{N}(0, \sigma^2)$. However, it is known that there exists k^* in $\mathbb{R}^{*+}$ verifying:

$$\frac{\alpha}{2} = k^*\sigma \tag{12}$$

and that from [23]:

$$P(|\theta| < k^*\sigma) = 2\phi(k^*) - 1 \tag{13}$$

where $\phi(.)$ is the cumulative distribution function of the standard normal law. Thus, the problem of finding σ^* is equivalent to finding $k^* \in \mathbb{R}^{*+}$ verifying:

$$2\phi(k^*) - 1 = P_D^{max} \tag{14}$$

Then, the value of σ verifying eq. (12) for the deduced value of k^* will be the solution σ^*. Note that the solution $k^* \in \mathbb{R}^{*+}$ for (14) can be easily found numerically using the quantile function of the standard normal distribution. Therefore, σ^* is deduced.

Now that σ^* is computed, for $\theta \in [-\alpha/2, \alpha/2]$, define the distribution:

$$\chi(\theta) = \frac{1}{\sigma^*\sqrt{2\pi}} e^{\frac{-\theta^2}{2\sigma^{*2}}} \tag{15}$$

which reflects the angular uncertainty of the sensor.

Finally, one can compute the probability of detection P_D:

$$P_D = \sum_{t \in \Gamma(T)} \int_{\Omega(t)} \chi(\theta)\ d\theta \tag{16}$$

In fact, (16) sums up the areas between the x-axis and the function χ over all the intervals $\Omega(t)$ for $t \in \Gamma(T)$. Thus, the methodology presented here involves not only the angular uncertainty but also the CS of the nearest target(s) as pointed out in subsection III-A. Illustrations of the methodology proposed for the computation of P_D associated to Fig. 2a-6a are given in Fig. 2b-6b respectively. In addition, the respective SM are illustrated in Fig. 2c-6c.

The modeling choice presented here follows the intuition from subsection III-A and has been validated in real experiments [22]. Note that other factors (e.g. further types of sensor noise, specular reflection, cross-talk) can be considered in the formulation of the SM but they are not treated in this section. In addition, for the sake of simplicity, the present formulation supposes that P_D^{max} does not depend on the distance to the detected obstacle. Without difficulty, a more realistic formulation would take into account the attenuation of P_D^{max} when the distance to the targets increases.

IV. Inverse Sensor Model Formulation

The ISM formulation for multi-target sensors based on the nearest-target hypothesis is now presented. The objective is to compute the probability of occupancy of each cell in the two-Dimensional (2D) grid $\mathcal{G}$ based on equations (2) and (4) and given measurement z.

To compute $p(z|s_i)$ for $i \in \{0, ..., N-1\}$ based on (4), one has to sum up $p(z|G_k^{s_i} \wedge s_i)$ over all possible grid configurations $G_k^{s_i}, k = 1, ..., 2^{N-1}$. However, using the nearest-target hypothesis, it can be noticed that different configurations might share the same value of $p(z|G_k^{s_i})$ for a certain value $k \in \{1, ..., 2^{N-1}\}$. In fact, two grids having the same set Γ will have the same SM. Thus, the sum in (4) can be reduced by "factorizing" these grid configurations. This is shown in the rest of this section.

Let us now introduce some notations used in the computation of $p(z|s(c_i))$. For $i \in \{0, ..., N-1\}$, denote $r(c_i)$ and $\Omega(c_i)$ the distance from cell c_i to the sensor and its CS, respectively. In the present study, the sensor is located at the origin of the grid and its principal axis corresponds to the y axis. Denote r_{min} the minimum of $\{r(c_i)\}_{i=0}^{N-1}$ and r_{max} its maximum. For $r \in [r_{min}, r_{max}]$, define the set $C(r) = \{c\ ;\ c \in \mathcal{G} \text{ and } r(c) = r\}$ representing the cells at distance r. Finally, for a set of cells A verifying the following criteria: "all the cells in A are at the same distance to the sensor denoted by $r(A) \in \mathbb{N}^*$", define $G(A)$ as a configuration grid where $\Gamma(G(A)) = A$. In other terms, all the cells which have a smaller range than $r(A)$ in $G(A)$ are empty, those having a range $r(A)$ are occupied if and only if they are in A, and the cells having a higher range than $r(A)$ cells can have any state (occupied or empty).

A. Computation of $p(z|o(c_i))$

Now, suppose that $s_i = o(c_i)$. One wants to compute $p(z|o(c_i))$ by applying (4). From the nearest-target hypothesis and because two grids that share the same set Γ have the same SM, one can proceed as follows. First, all the possible non empty sets composed of cells with the same distance to the sensor that is smaller or equal to $r(c_i)$ should be identified. Then, only the configuration grids having a set Γ that is equal to one of the identified sets are taken into account in the sum (4):

$$p(z|o(c_i)) = \sum_{r_{min} \le r \le r(c_i)} \sum_{A \in \mathcal{P}_r^{c_i}} p(z|G(A) \wedge o(c_i)) \cdot P(G(A)) \tag{17}$$

where $\mathcal{P}_r^{c_i}$ is the set of all the possible combinations of cells in $C(r)$ excluding cell c_i from these combinations and the empty selection if $r < r(c_i)$.

For a fixed distance $R \in [r_{min}, r(c_i)]$ and for $A \in \mathcal{P}_R^{c_i}$, the term $p(z|G(A) \wedge o(c_i))$ in (17) can be directly deduced from the SM. In fact, once $\Gamma(G(A) \wedge o(c_i))$ is known, one can proceed as in (7) and (16) to compute $p(z|G(A) \wedge o(c_i))$. However, $\Gamma(G(A) \wedge o(c_i))$ is equal to A if $r(A) < r(c_i)$, and it is equal to $A \cup c_i$ if $r = r(c_i)$. Therefore:

$$p(z|G(A) \wedge o(c_i)) = \kappa \tag{18}$$

where

$$\kappa = \frac{P_D}{\sigma_{r(A)}\sqrt{2\pi}} e^{\frac{-(z-r(A))^2}{2\sigma_{r(A)}^2}} + \frac{P_{MD}}{\hat{\sigma}\sqrt{2\pi}} e^{\frac{-(z-z_{max})^2}{2\hat{\sigma}^2}} \tag{19}$$

with

$$P_D = \begin{cases} \sum_{c \in A} \int_{\Omega(c)} \chi(\theta)\ d\theta & \text{if } r(A) < r(c_i) \\ \sum_{c \in A \cup c_i} \int_{\Omega(c)} \chi(\theta)\ d\theta & \text{if } r(A) = r(c_i) \end{cases} \tag{20}$$

Note that the size of each cell c in $\Gamma(G(A) \wedge o(c_i))$, its angular position and its distance to the sensor will play an interacting role in determining $\Omega(c)$ and then P_D.

Besides, $P(G(A))$ in (17) is equal to the probability of intersection of the following events:

1) all the cells at a distance smaller than R are empty. The probability of this event is denoted by $P_1^{R,A}$. It is equal to:

$$P_1^{R,A} = \prod_{c \in \bigcup_{r<R} C(r)} P(e(c)) \tag{21}$$

2) cells in A are occupied. The probability of this event is denoted by $P_2^{R,A}$. It is equal to:

$$P_2^{R,A} = \prod_{c \in A} P(o(c)) \tag{22}$$

3) cells in $C(R) \setminus (A \cup c_i)$ are empty. The probability of this event is denoted by $P_3^{R,A}$. It is equal to:

$$P_3^{R,A} = \prod_{c \in C(R) \setminus (A \cup c_i)} P(e(c)) \tag{23}$$

Thus, in this case $P(G(A)) = P_1^{R,A} \cdot P_2^{R,A} \cdot P_3^{R,A}$. Finally:

$$p(z|o(c_i)) =$$

$$\sum_{r_{min} \leq r \leq r(c_i)} \sum_{A \in \mathcal{P}_r^{c_i}} P_1^{r,A} \cdot P_2^{r,A} \cdot P_3^{r,A} \cdot p(z|G(A) \wedge o(c_i)) \tag{24}$$

B. Computation of $p(z|e(c_i))$

Suppose now that $s_i = e(c_i)$. Following the same reasoning as above, $p(z|e(c_i))$ is given by:

$$p(z|e(c_i)) = \sum_{r_{min} \leq r \leq r_{max}} \sum_{A \in \hat{\mathcal{P}}_r^{c_i}} p(z|G(A) \wedge e(c_i)) \cdot P(G(A)) \tag{25}$$

where $\hat{\mathcal{P}}_r^{c_i}$ in this case is the set of all the possible combinations of cells in $C(r)$ excluding cells c_i and the empty set for $r \leq r_{max}$. Since c_i is empty this time, the first occupied cell in the grid configurations used in (4) can be greater than $r(c_i)$. Note that this was not the case when c_i was occupied. This explains why the sum over r can reach r_{max} in (25). However, it should be smaller or equal to $r(c_i)$ in (17).

Similarly, for a fixed $R \in [r_{min}, r_{max}]$ and for $A \in \hat{\mathcal{P}}_R^{c_i}$, the term $p(z|G(A) \wedge e(c_i))$ in (25) can be deduced from the SM. This time, $\Gamma(G(A) \wedge e(c_i))) = A \ \forall r \in [r_{min}, r_{max}]$ and

$$p(z|G(A) \wedge e(c_i)) = \kappa \tag{26}$$

with κ in (19), and

$$P_D = \sum_{c \in A} \int_{\Omega(c)} \chi(\theta) \ d\theta \tag{27}$$

In addition, $P(G(A))$ is computed as above. However, cell c_i must be excluded when computing the probability ${P_1}^{R,A}$. Thus, a modified $\hat{P_1}^{R,A}$ is defined as follows:

$$\hat{P_1}^{R,A} = \prod_{c \in \cup_{r<R} C(r) \setminus \{c_i\}} P(e(c)) \tag{28}$$

In this case, $P(G(A)) = \hat{P_1}^{R,A} \cdot P_2^{R,A} \cdot P_3^{R,A}$. Hence:

$$p(z|e(c_i)) =$$

$$\sum_{r_{min} \leq r \leq r_{max}} \sum_{A \in \hat{\mathcal{P}}_R^{c_i}} \hat{P_1}^{r,A} \cdot P_2^{r,A} \cdot P_3^{r,A} \cdot p(z|G(A) \wedge e(c_i)) \tag{29}$$

C. Final Formulation of the ISM

By substituting equations (24) and (29) in (2), the Inverse Sensor Model is obtained.

In this paper, only probabilistic OGs are considered as a representation of the environment [13]. However, since a probablistic ISM for nearest-target sensors is given, the approach proposed is not restricted to OGs but can be useful in other representations where a probabilistic ISM is required such as the octomap representation [24].

V. Implementation of the Sectoral Decomposition

For a realistic implementation of the ISM, a uniform sectoral decomposition of the sensor FOV into B sections w_m, $m = 1, ..., B$ for $B \in \mathbb{N}^*$ is now considered. The new formulation of the ISM based on the sectoral decomposition is first detailed in subsection V-A. Then, the computational complexity is discussed in subsection V-B.

A. Formulation of the ISM based on the Sectoral Decomposition

The main motto is that, instead of taking into account all the possible cell state combinations at each distance $r \in [r_{min}, r_{max}]$ when (24) and (29) are computed, only the state combinations of $w_m^r, m = 1, ..., B$ are considered. Here, w_m^r represents the set of cells at distance r in sector w_m, i.e. $w_m^r = \{c \ ; \ c \in w_m \text{ and } r(c) = r\}$. w_m^r is considered occupied if there exists at least one occupied cell that belongs to it. Hereafter, the sectoral decomposition technique is detailed. The new expression of (24) derived from this technique is given. A similar approach can be applied to (29). However, due to space limitation, it is not reported in the paper.

For $m \in \{1, ..., B\}$ and $r \in [r_{min}, r_{max}]$, denote $o(w_m^r)$ the event that w_m^r is occupied and $e(w_m^r)$ if it is not. For a given set $T_r = \{s(w_1^r), ..., s(w_B^r)\}$ where $s(w_m^r) \in \{o(w_m^r), e(w_m^r)\}$ for $m \in \{1, ..., B\}$, define $G(T_r)$ as a configuration grid where $\Gamma(G(T_r)) = \{c \ ; \ c \in w_m^r \ \ m \in \{1, ..., B\}$ and $s(w_m^r) = o(w_m^r)\}$. Using the sectoral decomposition, $p(z|o(c_i))$ in (24) becomes:

$$p(z|o(c_i)) =$$

$$\sum_{r_{min} \leq r \leq r(c_i)} \sum_{T \in \mathcal{T}_r^{w(c_i)}} p(z|G(T) \wedge w((c_i))) \cdot P(G(T)) \tag{30}$$

where $\mathcal{T}_r^{w(c_i)}$ is the set containing all the possible state combinations of $w_m^r, m \in \{1, ..., B\}$ excluding $w(c_i)$, and $w(c_i)$ denotes the sector which contains cell c_i in the following set $\{w_m^{r(c_i)}, m \in \{1, ..., B\}\}$.

For a fixed distance $R \in [r_{min}, r(c_i)]$ and for $T \in \mathcal{T}_R^{w(c_i)}$, the term $p(z|G(T) \wedge w((c_i)))$ in (30) can be directly deduced from the SM:

$$p(z|G(T) \wedge w((c_i))) = \kappa \tag{31}$$

where

$$\kappa = \frac{P_D^{T,i}}{\sigma_R\sqrt{2\pi}} e^{\frac{-(z-R)^2}{2{\sigma_R}^2}} + \frac{P_{MD}^{T,i}}{\hat{\sigma}\sqrt{2\pi}} e^{\frac{-(z-z_{max})^2}{2\hat{\sigma}^2}} \quad (32)$$

In this case, $P_D^{T,i}$ is computed as before. The main difference is that the combined CS takes into account all cells in each occupied sector in T if $R < r(c_i)$ and all cells of $T \cup w(c_i)$ if $R = r(c_i)$.

Besides, $P(G(T))$ in (30) is equal to the probability of intersection of the following events:

1) all the cells at a distance smaller than R are empty. The probability of this event is denoted by $P_1^{R,T}$ and is equal to:
$$P_1^{R,T} = \prod_{c \in \cup_{r<R}\ C(r)} P(e(c)) \quad (33)$$
2) at least one cell is occupied in each occupied sector of T. The probability of this event is denoted by $P_2^{R,T}$ and is equal to:
$$P_2^{R,T} = \prod_{w;\ o(w)\in T} (1 - \prod_{c\in w} p(e(c))) \quad (34)$$
3) all cells in the empty sectors of T are empty. The probability of this event is denoted by $P_3^{R,T}$ and is equal to:
$$P_3^{R,T} = \prod_{c\in w;\ e(w)\in T} P(e(c)) \quad (35)$$

Thus, in this case $P(G(T)) = P_1^{T,A} \cdot P_2^{T,A} \cdot P_3^{T,A}$. Finally,

$$p(z|o(c_i)) = \frac{\sum_{r_{min}\le r\le r(c_i)} \sum_{T\in\mathcal{T}_r^{w(c_i)}} P_1^{r,T}\cdot P_2^{r,T}\cdot P_3^{r,T}\cdot p(z|G(T\wedge o(w((c_i)))))}{} \quad (36)$$

B. Computational Complexity

Applying the sectoral decomposition, the computation of $P(o_i|z), i \in 0, ..., N-1$ (respectively, $P(e_i|z)$) requires less than $\frac{N}{B}2^B$ operations because only the combination of B sectors is considered at each range. Therefore, the complexity is *linear* with respect to N.

The sectoral decomposition technique supposes that the Sensor Model generated by only one nearest occupied cell in a sector is identical if all the nearest cells in the sector are occupied. Note that when B increases, in a way that only one nearest occupied cell is located in each sector, the sectoral decomposition is equivalent to the exact formulation presented in sections III and IV and the complexity increases to reach the exponential one.

The interest in the sectoral decomposition lies in the fact that depending on the degree of detection required, one can tune the number of sectors in order to avoid unnecessary complex computations. This kind of trade-off can be useful when free space detection is considered. In that case, detection of occupied regions with a high precision is not crucial. As a consequence, one can choose small values of B, leading to a low-complexity computation. This approach also helps keeping the link between the SM and the ISM for multi-target sensors as discussed in section II-B (See table I).

VI. Test and Validation of the Sectoral Decomposition

The objective of this experiment is to demonstrate that the proposed ISM together with sectoral decomposition can be used in conjunction with scanning to precisely localize obstacles in the environment and assess free space.

A 2D uniform square grid of length $5m$ composed of cells of length $2cm$ is considered. The scene setup consists of two objects t_1 and t_2 placed in front of the sensor at different positions with distances $r_1 = 5m$ and $r_2 = 8m$, see Fig. 7a for the experiment setup. The sensor FOV is equal to $15°$.

Sixteen acquisitions have been performed with a clockwise shift of $1°$ of the sensor FOV (referred as to "scanning technique"), starting from the position where the principal axis of the sensor FOV is aligned with the y_0 axis of the grid, see Fig. 7a. Fig. 7b shows the occupancy grid obtained after the first, 6^{th} and last scans, when $B = 3$ sectors are considered. The right down picture of Fig. 7b is obtained by computing the Bayesian Fusion of all the 16 occupancy grids [25]. Note that both obstacles can be precisely localized thanks to the scanning even if only the nearest target is considered for each scan.

VII. Conclusion

In this paper, a new definition of the Sensor Model under the nearest-target hypothesis for multi-target sensors is proposed. The model takes into account the probability of detection of the nearest target(s) with respect to its (their) angular position in the sensor Field-Of-View, its (their) distance to the sensor and its (their) Cross Section.

In addition, the formulation of the Inverse Sensor Model directly derived from the proposed Sensor Model is given. This formulation keeps the link between the Sensor Model and its Inverse Sensor Model. Moreover, the Inverse Sensor Model formulation can be easily adapted to various types of sensors with different uncertainties in the Sensor Model.

Finally, an implementation of the Inverse Sensor Model developed in the present paper together with a sectoral decomposition of the sensor Field-Of-View is proposed. Using this technique, the computational complexity breaks down to a linear one, leading to a tractable computational implementation even for highly dense grids. The number of sectors has a direct influence on the computational load and on the capability to highlight the occupied space.

The proposed models are tested in a realistic simulation setup, showing the effectiveness of our solution.

References

[1] H. Moravec and A. Elfes, "High resolution maps from wide angle sonar," in *Proceedings. IEEE ICRA*, vol. 2, Mar 1985, pp. 116–121.
[2] J. Borenstein and Y. Koren, "The vector field histogram-fast obstacle avoidance for mobile robots," *IEEE Transactions on Robotics and Automation*, vol. 7, no. 3, pp. 278–288, 1991.
[3] S. P. Engelson and D. V. McDermott, "Error correction in mobile robot map learning," in *Robotics and Automation, 1992. Proceedings., 1992 IEEE International Conference on*. IEEE, 1992, pp. 2555–2560.
[4] D. Kortenkamp and T. Weymouth, "Topological mapping for mobile robots using a combination of sonar and vision sensing," in *AAAI*, vol. 94, 1994, pp. 979–984.

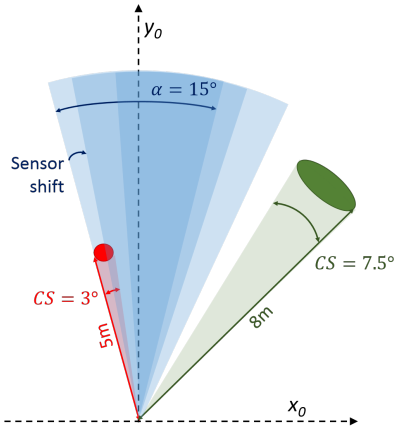

(a) Scene setup

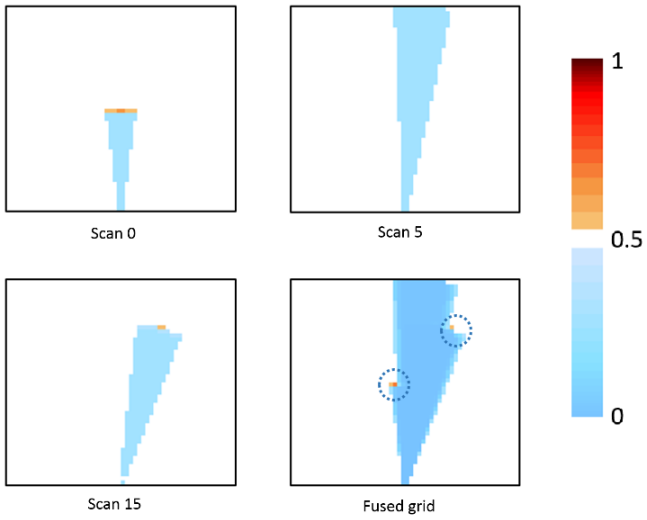

(b) Resulting scans and OG

Fig. 7: Results of 3 particular scans (first, sixth and last scan) and the Bayesian fusion of all the scans.

[5] A. Elfes, "Occupancy grids: A probabilistic framework for robot perception and navigation," Ph.D. dissertation, Carnegie Mellon University, Pittsburgh, PA, USA, 1989.

[6] G. Shafer, "The combination of evidence," *School of Business, University of Kansas, Lawrence, KS 66045*, 1986.

[7] M. Ribo and A. Pinz, "A comparison of three uncertainty calculi for building sonar-based occupancy grids," *Robotics and autonomous systems*, vol. 35, no. 3, pp. 201–209, 2001.

[8] S. Thrun, W. Burgard, and D. Fox, *Probabilistic Robotics (Intelligent Robotics and Autonomous Agents)*. The MIT Press, 2005.

[9] P. Stepan, M. Kulich, and L. Preucil, "Robust data fusion with occupancy grid," *IEEE Transactions on Systems, Man, and Cybernetics, Part C (Applications and Reviews)*, vol. 35, no. 1, pp. 106–115, 2005.

[10] R. Dia, J. Mottin, T. Rakotovao, D. Puschini, and S. Lesecq, "Evaluation of occupancy grid resolution through a novel approach for inverse sensor modeling," in *IFAC World Congress*, 2017.

[11] K. Pathak, A. Birk, J. Poppinga, and S. Schwertfeger, "3d forward sensor modeling and application to occupancy grid based sensor fusion," in *Intelligent Robots and Systems, 2007. IROS 2007. IEEE/RSJ International Conference on*. IEEE, 2007, pp. 2059–2064.

[12] E. Kaufman, T. Lee, Z. Ai, and I. S. Moskowitz, "Bayesian occupancy grid mapping via an exact inverse sensor model," in *American Control Conference (ACC), 2016*. American Automatic Control Council (AACC), 2016, pp. 5709–5715.

[13] A. Elfes, "Occupancy grids: a stochastic spatial representation for active robot perception," *Sixth Conference on Uncertainty in AI*, 1990.

[14] S. Thrun, "Learning occupancy grid maps with forward sensor models," *Autonomous robots*, vol. 15, no. 2, pp. 111–127, 2003.

[15] *M16 from LeddarTech*, accessed February 5, 2018. [Online]. Available: https://leddartech.com/modules/m16-multi-element-sensor-module/

[16] *Vu8 from LeddarTech*, accessed February 5, 2018. [Online]. Available: https://leddartech.com/modules/leddarvu/

[17] *VL53L0X from STM*, accessed February 5, 2018. [Online]. Available: http://www.st.com/en/imaging-and-photonics-solutions/vl53l0x.html

[18] *TeraRanger One from Terabee*, accessed February 5, 2018. [Online]. Available: https://www.terabee.com/portfolio-item/teraranger-one/

[19] *BGT24Axx*, accessed February 5, 2018. [Online]. Available: https://www.infineon.com/cms/en/product/rf-wireless-control/mmwave-mmic-transceivers-24-86-ghz/24ghz-radar-automotive/

[20] *AURIX*, accessed February 5, 2018. [Online]. Available: https://www.infineon.com/cms/en/product/microcontroller/32-bit-tricore-microcontroller/

[21] *cocoon radar from NXP*, accessed February 5, 2018. [Online]. Available: https://community.nxp.com/docs/DOC-334985

[22] XXX, "Validation of an occupancy model for multi-target sensors based on the nearest-target hypothesis," in *ommitted for blind review, DAC*, 2018.

[23] N. V. Smirnov and I. Dunin-Barkowski, "Mathematische statistik in der technik," 1963.

[24] A. Hornung, K. M. Wurm, M. Bennewitz, C. Stachniss, and W. Burgard, "Octomap: An efficient probabilistic 3d mapping framework based on octrees," *Autonomous Robots*, vol. 34, no. 3, pp. 189–206, 2013.

[25] T. Rakotovao, J. Mottin, D. Puschini, and C. Laugier, "Multi-Sensor Fusion of Occupancy Grids based on Integer Arithmetic," in *ICRA 2016 - IEEE International Conference on Robotics and Automation*, Stockholm, Sweden, May 2016.